53A_{del} = $f(\tau)$ for constant t_{sf}figure.caption.6 $forconstant\tau$ = 1 and ζM_* = 1238The $SFR_{0,del}$ and $\overline{SFR_{del}}$ for constant τ = 1 and ζM_* = 1figure.caption.25 τ_g with the SFR and the Stellar mass τ_g with the total mass and the mass of the gas τ_g with the color index τ_g with the color index

Investigations of the galaxies of the LCV

Dimitrios Papachistopoulos

June 10, 2023

0.1 TODO **no indent**

0.2 TODO **fullstops**

0.3 TODO **Units in the plots**

Abstract

The paper investigates the properties of galaxies in the Local Cosmological Volume (LCV), using the Catalogue of Neighboring Galaxies[2] and its updated version from the "Catalog & Atlas of the LV galaxies" database[1]. The properties studied include the galaxy types, their various masses, the star formation rates (SFRs) and the star formation timescale τ, gas depletion timescale τ_g and the star formation time t_{sf}. The paper aims to understand the distribution and correlation of these properties in the sample of galaxies in the LCV, and how they relate to current astrophysical theories.

1 The Galaxies in the Local Cosmological Volume (LCV)

The Catalogue of Neigbouring Galaxies (Karachentsev, Igor D. and Makarov et al. 2013[2]) and its updated version from the "Catalog & Atlas of the LV galaxies" database[1] are used to extract the B-band, FUV \ K-band luminosities[1] , the types of the galaxie[2]s, the mass within the Holmberg radius (M26), the Hydrogen masses of the galaxies (M_{HI}) and the SFRs based on integrated H and far-ultraviolet (FUV) measurments for galaxies within a distance of ≈ 11 Mpc. Some of those values contain limit flags, which we exclude from our present analysis. This gives a sample of 793 galaxies from 1248. From the remaing galaxies we have

Measurment	Number of Galaxies
Name	793
FUVmag	687
TType	793
Tdw1	580
Tdw2	568
Bmag	790
SFR_{Ha}	566
SFR_{FUV}	688
K	789
MHI	643
color	686

The K-band values are converted to the total Stellar Masses of each galaxy according to the mass-to-light ratio of 0.6 ([5]), and the M_{HI} can be converted to the total mass of the gas of the galaxy using the equation $M_g = 1.33\, M_{HI}$

The total SFR of each galaxy can be calcuated by

$$SFR_o = \frac{SFR_{FUV} + SFR_{Ha}}{2}$$

if both $SFR_{H\alpha}, SFR_{FUV}$ measurments are available. If only one only one of them is given, then the SFR is equal to the given SFR value

$$SFR_o = SFR_i, \text{ if } SFR_j = 0, i \neq j,\ i,j = FUV, H_a$$

[1] We use the FUV and B measurments to calculate the <FUV-B> color index.

[2] TType=Morphology type code according to the classification by de Vaucouleurs/ Tdw1=Dwarf galaxy morphology/ Tdw2=Dwarf galaxy surface brightness morphology

The condition $SFR_o \geq 10^{-3} M_{\odot} yr^{-1}$ leaves 579 galaxies. This condition is applied due to the reasons given in the P. Kroupa,M. Haslbauer, I. Banik, S. T. Nagesh and J. Pflamm-Altenburg et al. 2020 [4]

2 Types of galaxies

Using the dataset of 1248 galaxies, do before using the condition and removing the galaxies with the flags, the below histograms can be plotted.

Most of the galaxies in the LCV are Irregular galaxies followed by lenticular galaxies

Out of the 1248 galaxies the 1022 are dwarf galaxies

2.1 TODO write a table with the types

Most dwarf galaxies have low brightness and are irregulars followed by Dwarf spheroidal.

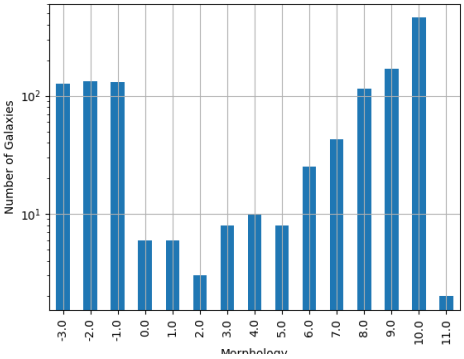

Figure 1: The classification by de Vaucouleurs et al. (1991) is used for the morphology of the galaxies

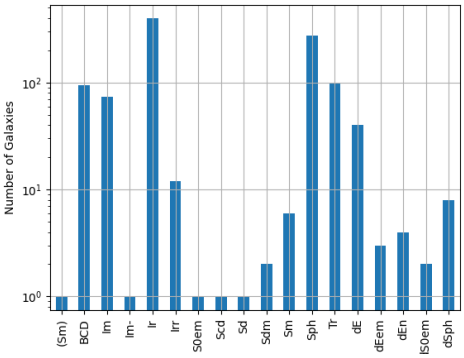

Figure 2: Dwarf galaxy morphology

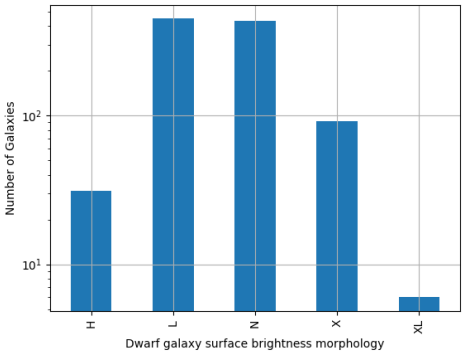

Figure 3: Dwarf galaxy surface brightness morphology, where: H = high; N = normal; L = low; X = extremely low.

3 Delayed-τ model

According to P. Kroupa et al. 2020[4] current star formation rates of galaxies can be described by the 'delayed-τ' model as

$$SFR_{0,del} = \frac{A_{del} x e^{-x}}{\tau}, \text{ where } x = \frac{t_{sf}}{\tau} \quad (1)$$

where τ is the star formation time-scale, t_{sf} is the real time of star formation in a given galaxy and A_{del} a normalization constant.

The average SFR is

$$\overline{SFR_{del}} = \frac{A_{del}}{t_{sf}}[1 - (1+x)e^{-x}] \quad (2)$$

and can also be defined by the present day stellar mass

$$\overline{SFR} = \frac{\zeta M_*}{t_{sf}} \quad (3)$$

where ζ accommodates for mass-loss through stella evolution and $\zeta \approx 1.3$

This is a system of 2 equations and 3 variables, since A_{del} has never been calculated

3.1 Constant t_{sf}

The observed ages of galactic discs are $t_{sf} \approx 12$ Gyr[3], so assuming an approximation of $t_{sf} = 12.5$ Gyr, the $\overline{SFR_{del}}$ can be calcuated, from the equation (3).

After that the equation of ratio

$$\frac{\overline{SFR_{del}}}{\overline{SFR_{0,del}}} = \frac{e^x - x - 1}{x^2} \quad (4)$$

can be solved numerically for x and using the equations (1) and (2) the A_{del} and τ of each galaxy are found.

	A_{tsf}	tau	x_{tsf}
count	578	579	579
mean	2.24715e+12	1.08958e+11	1.853
std	3.93675e+13	1.04132e+12	1.476
min	2.47798e+07	1.93205e+09	0.001
25%	1.40573e+08	4.18098e+09	0.565
50%	6.83764e+08	7.79265e+09	1.604
75%	5.70379e+09	2.21327e+10	2.99
max	9.10088e+14	2.23774e+13	6.47

$\log(A_{del}|_{tsf}) = (9.6(4) \times 10^{-1}) \cdot \log(M_t)$ + (8(4) $\times 10^{-1}$) with correlation $R^2 = 48\%$ (5)

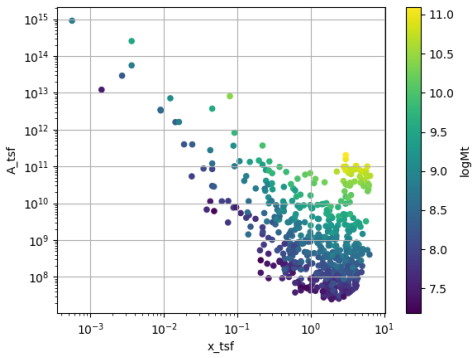

Figure 4: $A_{del} = f(x)$ for constant t_{sf}

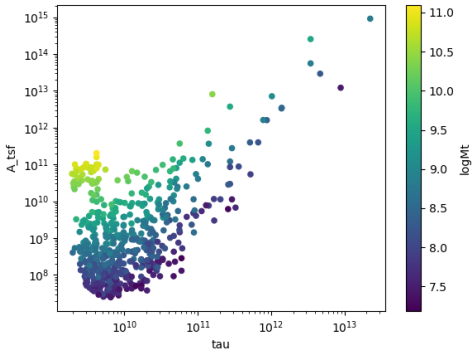

Figure 5: $A_{del} = f(\tau)$ for constant t_{sf}

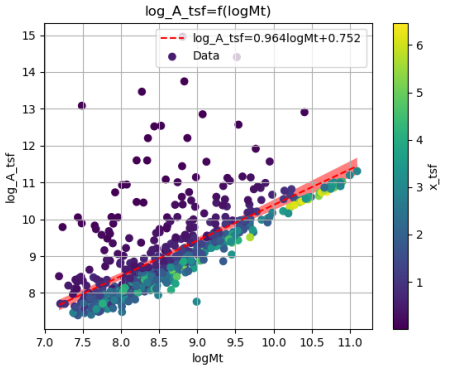

Figure 6: Total Mass M_t - $A_{del}|_{t_{sf}}$

3.2 Constant τ

Assuming for an constant $\tau = 3.5$ Gyr, we cannot use the same $\overline{SFR}$ since it depends on t_{sf}. Using the equations~(3) and (4)

$$\frac{\overline{SFR_{del}}}{SFR_{0,del}} = \frac{e^x - x - 1}{x^2} \Leftrightarrow \frac{e^x - x - 1}{x} = \frac{\zeta M_*}{SFR \cdot \tau}$$

using this equation x and A_{del} can be calculated numerically.

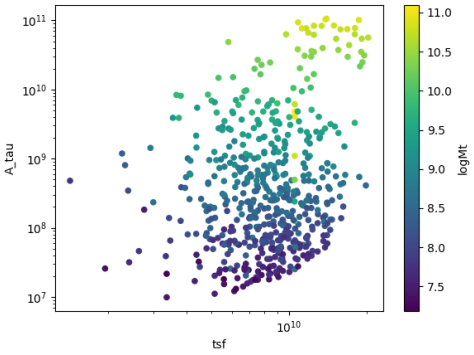

Figure 8: $A_{del} = f(t_{sf})$ for constant τ

	A_{tau}	x_{tau}	ts
count	579	579	579
mean	4.58667e+09	2.54057	8.89201e+09
std	1.49896e+10	0.956554	3.34794e+09
min	9.87003e+06	0.406787	1.42376e+09
25%	6.50497e+07	1.87165	6.55079e+09
50%	2.36667e+08	2.43871	8.5355e+09
75%	1.11526e+09	3.07972	1.0779e+1(
max	1.0577e+11	5.77102	2.01986e+1(

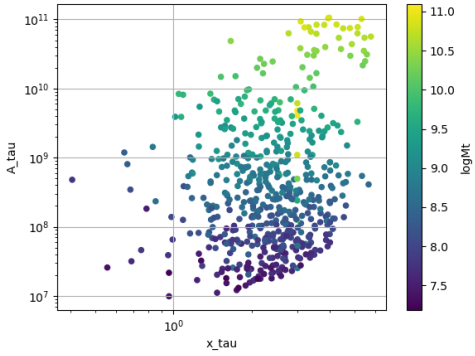

Figure 7: $A_{del} = f(x)$ for constant τ

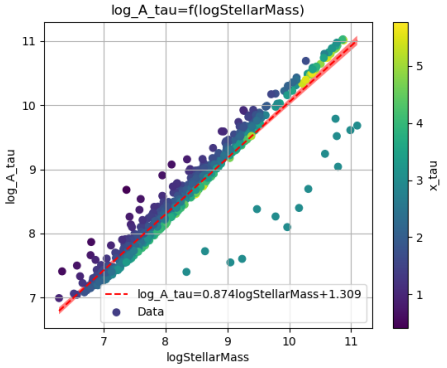

Figure 9: Total Mass M_t - $A_{del}|_\tau$

$\log(A_{del}|_\tau) = (8.74(12) \times 10^{-1}) \cdot \log(M_t) + (1.31(10) \times 10^0)$
with correlation $R^2 = 90\%$ (6)

	x_tau	x_tsf
count	5.79E+02	5.79E+02
mean	2.54E+00	1.85E+00
std	9.57E-01	1.48E+00
min	4.07E-01	5.59E-04
25%	1.87E+00	5.65E-01
50%	2.44E+00	1.60E+00
75%	3.08E+00	2.99E+00
max	5.77E+00	6.47E+00

3.3 Comparing the two results

3.3.1 Comparing the x's

Comparing the two different results for x, we see that the $x|_\tau$ has a lower σ

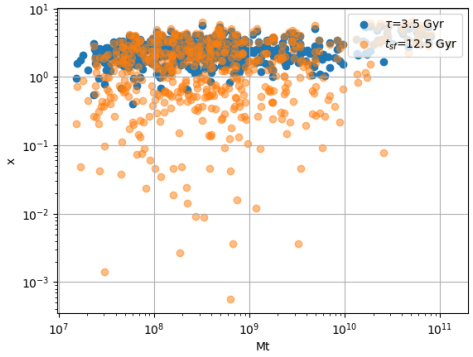

Figure 10: Comparing the two x's, According to their total masses

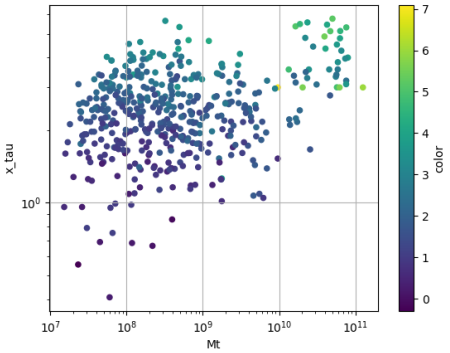

Figure 11: $x|_\tau = f(M_t)$, with their color index

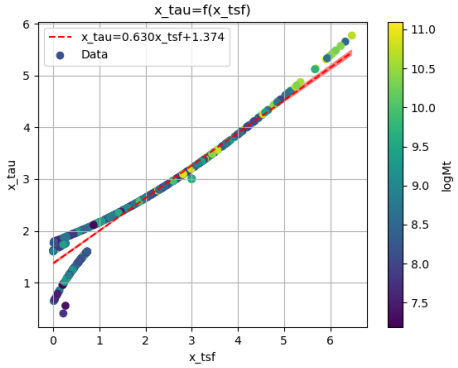

Figure 12: Comparing the two x, according to their total mass

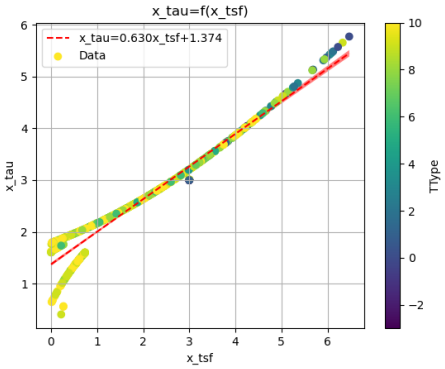

Figure 13: Comparing the two x, according to their type

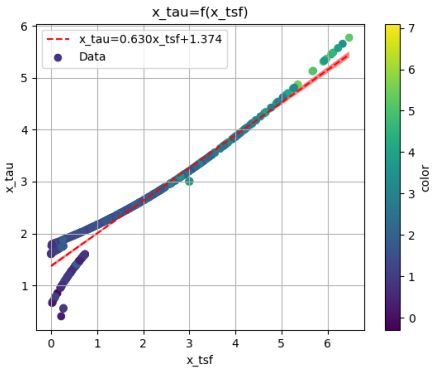

Figure 14: Comparing the two x, according to their color index

The two results are interrelated through the equation:

$$x|_\tau = (6.30(6) \times 10^{-1}) \cdot x|_{tsf} + (1.374(15) \times 10^{0})$$
$$\text{with correlation } R^2 = 94\% \tag{7}$$

and from the plots the following conclusions can be drawn:

1. The galaxies with a higher total mass deviate less from the linear fit and are older.
2. The younger galaxies are mainly later types of galaxies
3. For lower x's, the galaxies have a lower color index which indicates that they are younger. So the values are inline with the experimental values.

3.3.2 Comparing the normalization constants

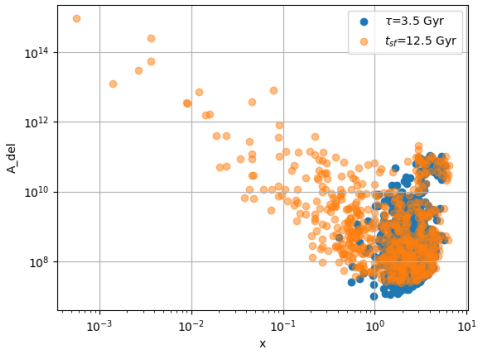

Figure 15: Comparing the two A_{del}

For high x and high masses the two A_{del}s have a high correlation. Specifically:

1. For high x the $A_{del}|_\tau - A_{del}|_{t_{sf}}$ plot follows a $y = x$ trend, which means that for older stars and stars with a low star formation timescale τ, the normalization constant is the same despite the method used to calculate it.
2. The same is true for more massive galaxies, since they deviate less from the $y = x$ line

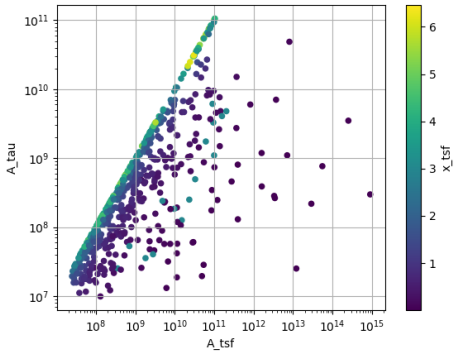

Figure 16: Comparison of the 2 A_{del}s according to their x

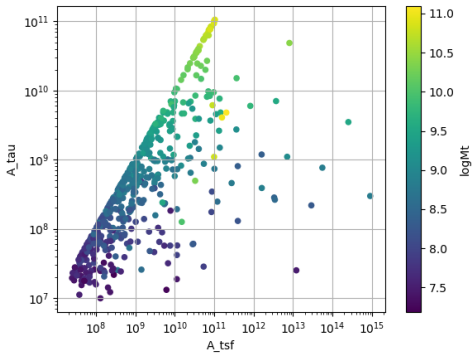

Figure 17: Comparison of the 2 A_{del}s according to their total masses

3.3.3 Trying to make the A_{del} cloud more compact

Having found $x|_{t_sf}$ and $x|_{\tau}$ we can find a relation between these two values

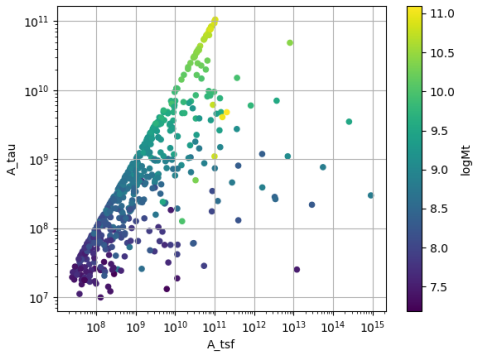

Figure 18: Comparison of the 2 A_{del}s according to their total masses

3.4 Int SFR to find the A_{del}

If we integrate equation (1) we get:

$$\int_0^{t_{sf}} SFR_{del} dt_{sf} = \int_0^{t_{sf}} \frac{A_{del} t_{sf} e^{-t_{sf}/\tau}}{\tau^2} dt_{sf}$$

$$\zeta \cdot M_* = -A_{del} \frac{(t_{sf}\tau + \tau^2) e^{\left(-\frac{t_{sf}}{\tau}\right)}}{\tau^2} + A_{del}$$

$$\zeta \cdot M_* = -A_{del} \frac{\tau^2 (x+1) e^{-x}}{\tau^2} + A_{del}$$

$$\zeta \cdot M_* = A_{del}(1 - (x+1)e^{-x})$$

$$A_{del} = \zeta \cdot M_* \frac{e^x}{e^x - x - 1} \tag{8}$$

The integral $\int SFR dt =$ The total mass that is turned into stars. But during the evolution of the stars, the stars spew mass to Interstellar space, so the galaxies lose mass during this process. So the observed Stellar Mass M_* is smaller than the total mass turned into Stellar Mass.

The constant ζ accommodates for this mass-loss and, as discussed earlier, we can assume a conservative value of 1.3 for the galaxies in the LCV.

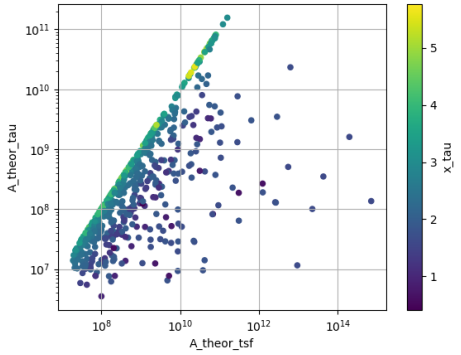

Figure 19: Comparison of the 2 A_{del}s according to their total masses

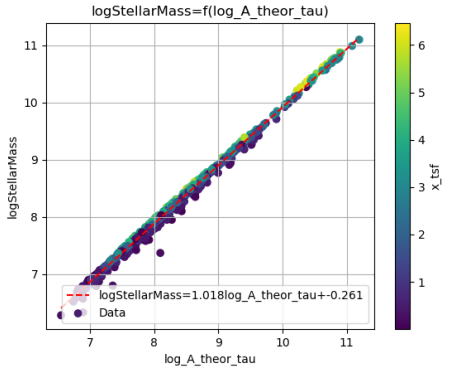

Figure 20: Comparison of the A_{del} according to their Stellar Mass

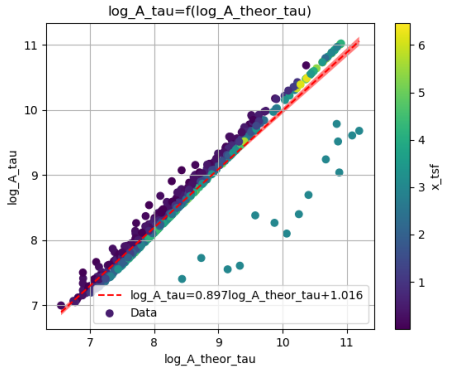

Figure 21: Comparison of the 2 $A_{del}|_{\tau=const.}$s (theoretical and experimental)

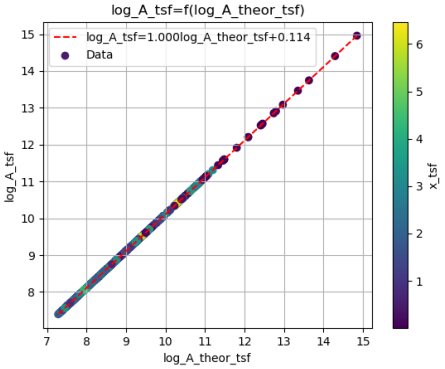

Figure 22: Comparison of the 2 $A_{del} | _{tsf=const.}$s (theoretical and experimental)

From the plots [**fig:A_theor_A_exp_tau**] and [**fig:A_theor_A_exp_tsf**] we get correlations of $R^2 = 91\%$ and $A_{tsf} = (8.97(12) \times 10^{-1}) \cdot A_{tsf,theor} + (1.02(10) \times 10^{0})$ so the theoretical values fit the experimental.

From the equations (1), (2) and (8), the $SFR_{0,del}$ and the $\overline{SFR_{del}}$ are given by the equations:

$$\begin{aligned} SFR_{0,del} &= \zeta M_* \frac{e^x}{e^x - x - 1} \frac{x e^{-x}}{\tau} \\ &= \zeta M_* \frac{x}{\tau(e^x - x - 1)} \end{aligned} \tag{9}$$

$$\begin{aligned} \overline{SFR_{del}} &= \zeta M_* \frac{e^x}{e^x - x - 1} \frac{1}{t_{sf}} [1 - (1 + x)e^{-x}] \\ &= \zeta M_* \frac{e^x}{e^x - x - 1} \frac{1}{t_{sf}} \frac{e^x - x - 1}{e^x} \\ &= \zeta \frac{M_*}{t_{sf}} \end{aligned} \tag{10}$$

The new $\overline{SFR_{del}}$ is the same with the $\overline{SFR}$ of the equation (3).

3.5 Calculating the t_{sf} and τ for each galaxy

Having found an expression for the A_{del}, we have eliminated on out of the 3 variables and now the t_{sf} and τ of each galaxy can be calculated.

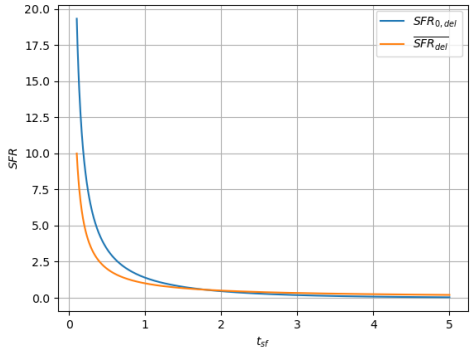

Figure 23: The $SFR_{0,del}$ and $\overline{SFR_{del}}$ for constant $\tau = 1$ and $\zeta M_* = 1$

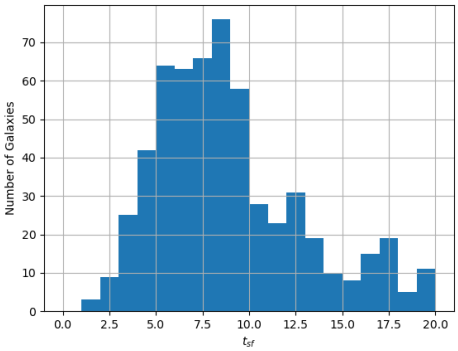

Figure 24: Histogram of t_{sf} from 0 to 20 Gyr

	tsfG	tauG	x
count	579	579	579
mean	9.047	3.429	2.548
std	4.637	1.197	0.849
min	1.307	1.262	0.642
25%	6.066	2.954	1.99
50%	8.238	3.297	2.467
75%	11.007	3.691	2.962
max	62.635	27.605	9.487

	tsfG2	tauG2	x2
count	579	579	579
mean	27.005	9.848	2.743
std	112.566	41.066	0
min	0.523	0.191	2.738
25%	4.329	1.578	2.743
50%	7.345	2.678	2.743
75%	14.071	5.13	2.743
max	1439.37	525.624	2.743

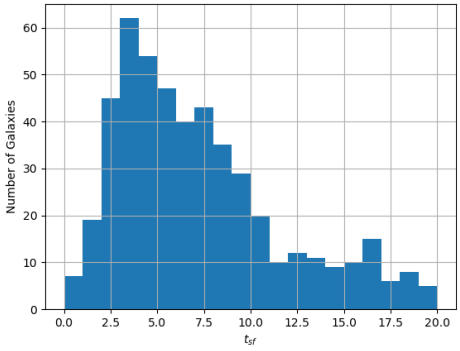

Figure 25: Histogram of t_{sf} from 0 to 20 Gyr

3.5.1 [?]

- Can we calculate/observe ζ?
  - If not: for galaxies with extreme star-bursting and low-metallicity galaxies $\zeta = 2 - 3$. Can we find those galaxies and approximate the ζ?
- Why couldn't we use (3) to calculate A_{del}
- While in the second method we see a better correlation between the age of the galaxy and the color index, we must have an older universe

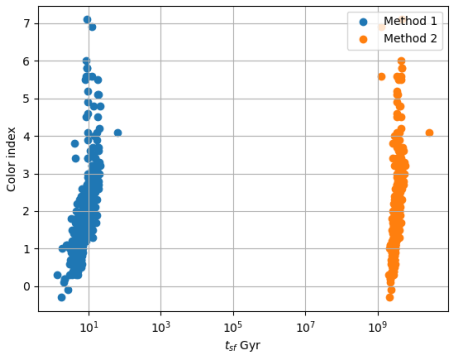

Figure 26: Comparing the two t_{sf}

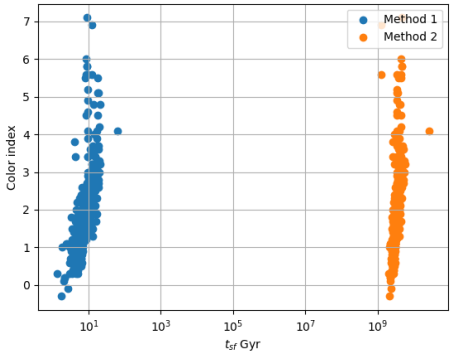

Figure 27: Comparing the two t_{sf}

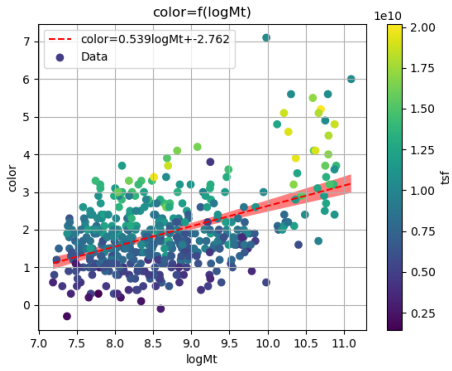

Figure 28: Comparison of the 2 $A_{del} | _{tsf=const.}$s (theoretical and experimental)

4 The gas depletion timescale τ_g

The gas depletion timescale τ_g measures the time taken by a galaxy to exhaust its gas content Mg given the current SFR[6, 7].

$$\tau_g = \frac{M_g}{\dot{M}_*} = \frac{M_g}{SFR} \tag{11}$$

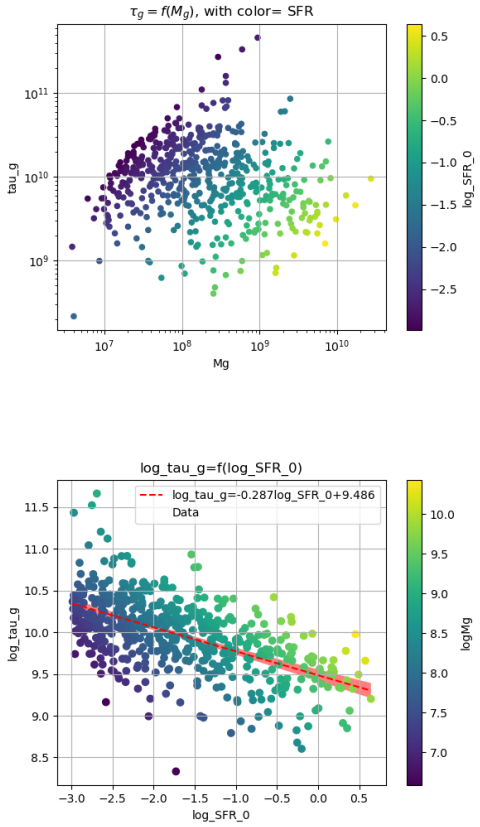

Figure 29: Correlation of the τ_g with the SFR and the gas mass

Despite a weak logarithmic correlation (as indicated by $R^2 = 32\%$), there is a noticeable trend of decreasing τ_g with increasing SFR and M_g.

The logarithmic correlation between $\tau_g - M_*$ is low ($R^2 = 21\%$), there seems to be a pattern wherein the decrease of τ_g corresponds to an increase in the values of the Stellar Mass, but there does not seem to be one for $\tau_g - \tau$

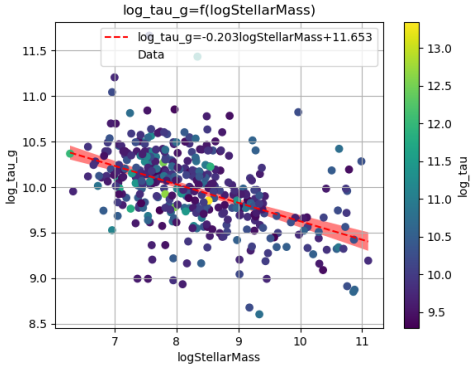

Figure 30: Correlation of the τ_g with the SFR and the Stellar mass

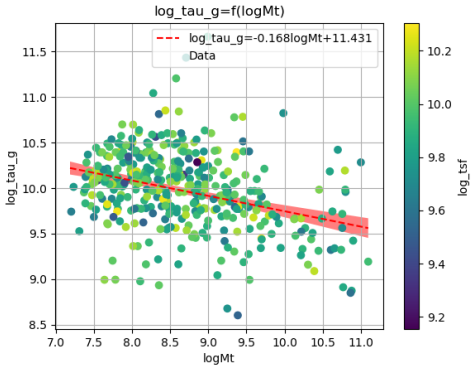

Figure 31: Correlation of the τ_g with the total mass and the mass of the gas

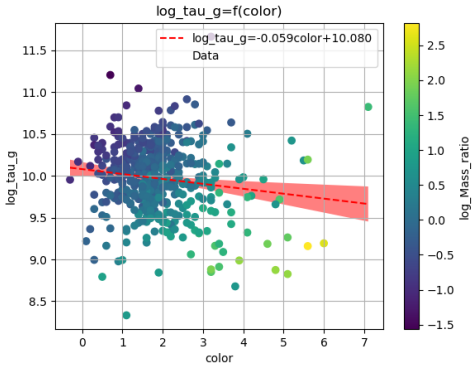

Figure 32: Correlation of the τ_g with the color index

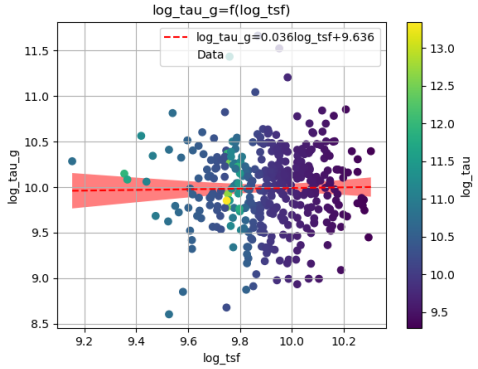

Figure 33: Correlation of the τ_g with the color index

Again it can be observed that as the τ_g decreases, the corresponding values of M_t increase, but the logarithmic correlation is again low ($R^2 = 11\%$), and there is no clear correlation between $\tau_g - t_{sf}$

There is a notable trend, wherein for high masses we have a shorter timescale.

5 Mass relations

Many of the galaxies masses have a high correlation with each other, and also help us understand the previous calculations.

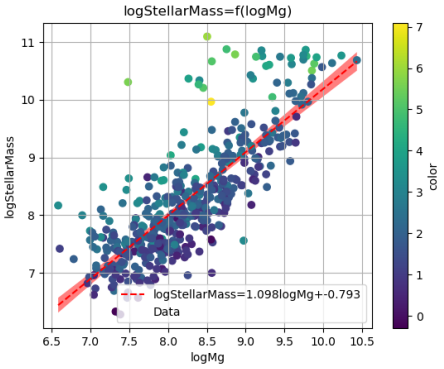

Figure 34: Gas Mass-Stellar Mass plot

For the plot 34:

M_g = (1.098(35) $\times 10^0$)·M_* + (-7.9(2.9) $\times 10^{-1}$)
with correlation $R^2 = 64\%$

(12)

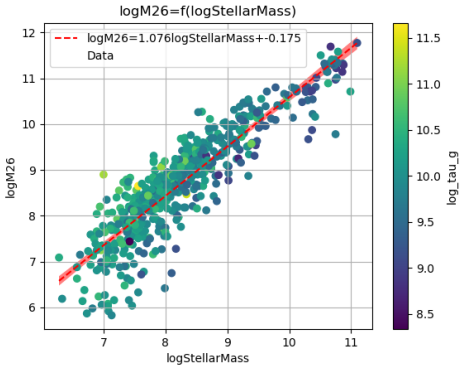

Figure 35: Mass inside the Holmberg radius-Stellar Mass plot

For the plot 35:

$M26 = (1.076(23) \times 10^0) \cdot M* + (-1.8(1.9) \times 10^{-1})$
with correlation $R^2 = 80\%$

(13)

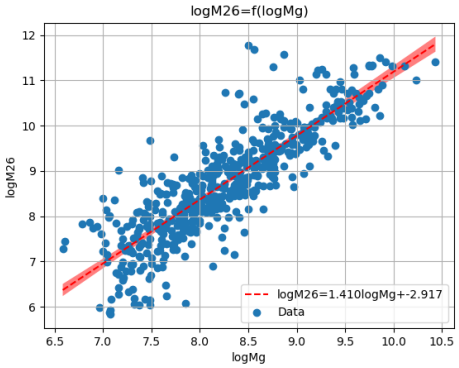

Figure 36: Mass inside the Holmberg radius-Gas Mass plot

For the plot 36:

$M26 = (1.41(4) \times 10^0) \cdot Mg + (-2.92(30) \times 10^0)$
with correlation $R^2 = 74\%$

(14)

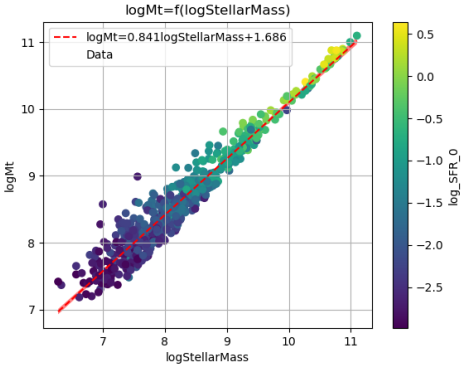

Figure 37: Stellar Mass-Total Mass plot

For the plot 37:

$$\mathrm{M}_t = (8.41(9)\times10^{-1})\cdot\mathrm{M}_* + (1.69(8)\times10^{0}) \quad \text{with correlation } R^2 = 94\% \tag{15}$$

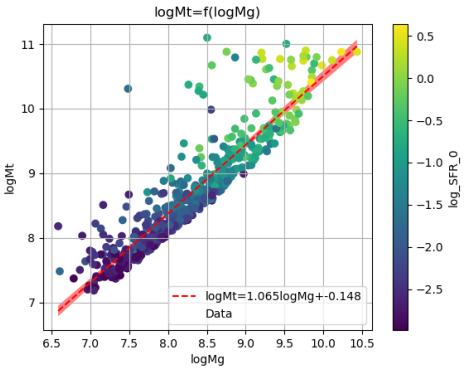

Figure 38: Total Mass - Gas Mass plot

For the plot 38:

$$\mathrm{M}_t = (1.065(23)\times10^{0})\cdot\mathrm{M}_g + (-1.5(1.9)\times10^{-1}) \quad \text{with correlation } R^2 = 81\% \tag{16}$$

$$M26 = (6.64(12)\times10^{-1})\cdot\mathrm{M}_t + (2.85(11)\times10^{0}) \quad \text{with correlation } R^2 = 85\% \tag{17}$$

There are many plots exhibiting a correlation of $R^2 > 80$

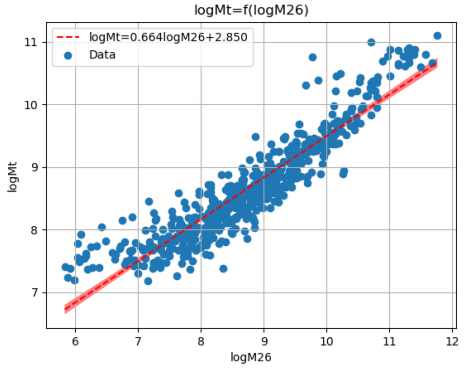

Figure 39: Mass inside the Holmberg radius-Total Mass plot

The $M_t - M_*$ (37) plot is particularly noteworthy, displaying a correlation of $R^2 = 94\%$. This plot also indicates that galaxies with greater total and stellar masses tend to have higher SFR, consistent with the findings in section 4 where τ_g decreases with increasing masses.

This phenomenon is likely due to the fact that galaxies with higher masses possess greater potential energy, which accelerates the star formation process. The galaxies with a high Mass ratio M_r could also help the process due to their dense regions and the resulting strong local gravitational potential.

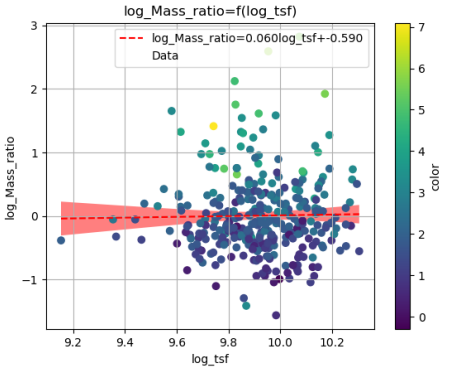

From the **??**, we conclude that when the color index is higher the Mass ratio decreases, which is to be expected, since the higher the B-FUV the more active the star formation of the galaxy.

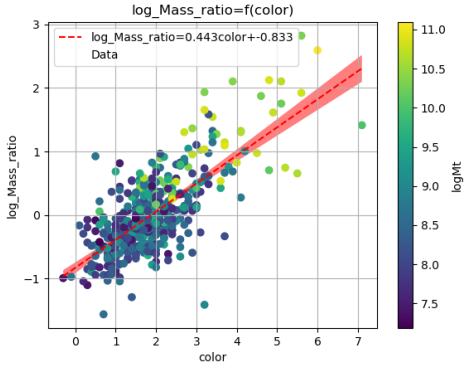

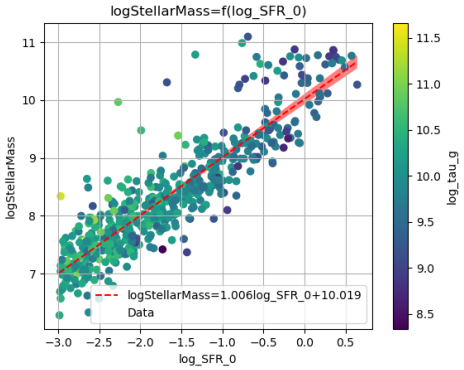

Figure 43: None

6 Variations in Star Formation Rate Across the Different Masses

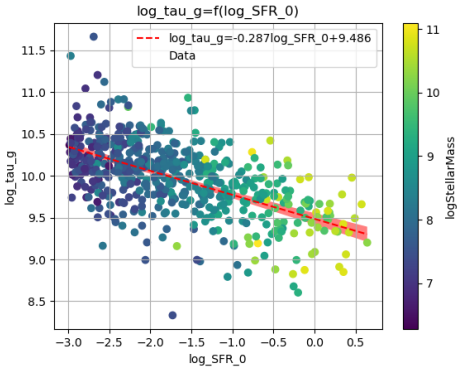

Figure 44: None

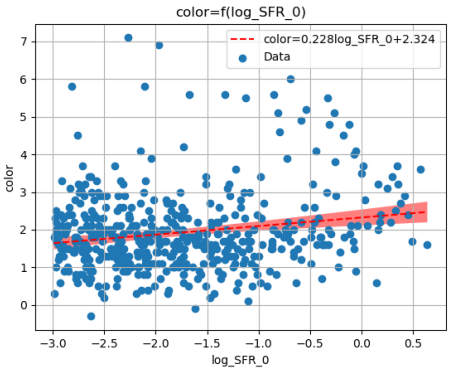

Figure 42: None

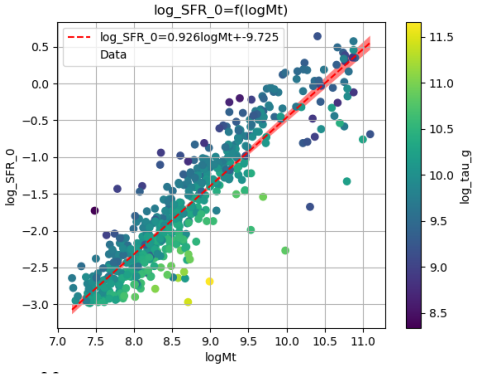

Figure 45: None

(<statsmodels.regression.linear_model.RegressionResul object at 0x7fbf61cc5a10>, '#+name: fig:None #+caption:None#+ATTR_LATEX: :placement [!htpb]

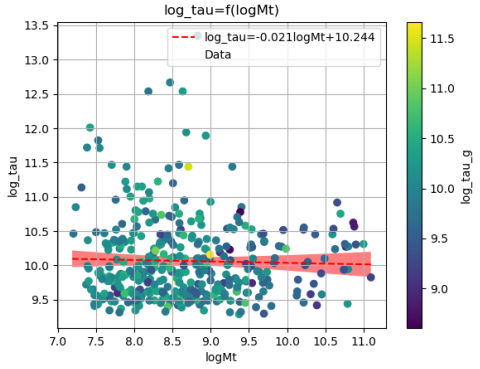

', 'logMt-$\log_{tau}$-$\text{color}_{logtaug}$')

(<statsmodels.regression.linear_model.RegressionResultsWrapper object at 0x7fbf61ee6b10>, '#+name: fig:None #+caption:None#+ATTR_LATEX: :placement [!htpb]

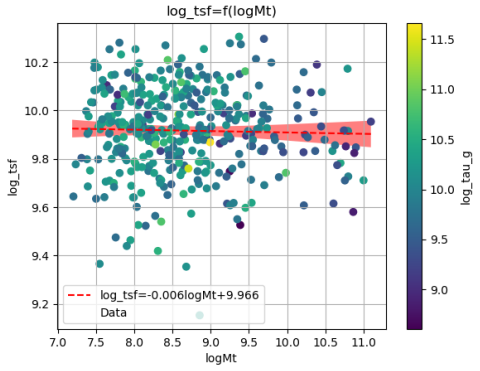

', 'logMt-$\log_{tsf}$-$\text{color}_{logtaug}$')

6.1 TODO **put that tau and tsf dont have a correlation with Mt**

References

[1] *Catalog of the LV Galaxies*. https://www.sao.ru/lv/lvgdb/tables.php. (Visited on 03/13/2023).

[2] Igor D. Karachentsev, Dmitry I. Makarov, and Elena I. Kaisina. "UPDATED NEARBY GALAXY CATALOG". In: *AJ* 145.4 (Mar. 2013), p. 101. ISSN: 0004-6256, 1538-3881. DOI: 10.1088/0004-6256/145/4/101. (Visited on 03/13/2023).

[3] R. A. Knox, M. R. S. Hawkins, and N. C. Hambly. "A Survey for Cool White Dwarfs and the Age of the Galactic Disc". In: *Monthly Notices of the Royal Astronomical Society* 306.3 (July 1999), pp. 736–752. ISSN: 0035-8711. DOI: 10.1046/j.1365-8711.1999.02625.x. (Visited on 03/13/2023).

[4] P Kroupa et al. "Constraints on the Star Formation Histories of Galaxies in the Local Cosmological Volume". In: *Monthly Notices of the Royal Astronomical Society* 497.1 (Sept. 2020), pp. 37–43. ISSN: 0035-8711. DOI: 10.1093/mnras/staa1851. (Visited on 03/13/2023).

[5] Federico Lelli, Stacy S. McGaugh, and James M. Schombert. "SPARC: MASS MODELS FOR 175 DISK GALAXIES WITH SPITZER PHOTOMETRY AND ACCURATE ROTATION CURVES". In: *AJ* 152.6 (Nov. 2016), p. 157. ISSN: 1538-3881. DOI: 10.3847/0004-6256/152/6/157. (Visited on 03/13/2023).

[6] Srikanth T. Nagesh et al. "Simulations of Star-Forming Main-Sequence Galaxies in Milgromian Gravity". In: *Monthly Notices of the Royal Astronomical Society* 519 (Mar. 2023), pp. 5128–5148. ISSN: 0035-8711. DOI: 10.1093/mnras/stac3645. (Visited on 03/13/2023).

[7] Jan Pflamm-Altenburg and Pavel Kroupa. "The Fundamental Gas Depletion and Stellar-Mass Buildup Times of Star Forming Galaxies". In: *ApJ* 706.1 (Nov. 2009). Comment: accepted for publication in ApJ, pp. 516–524. ISSN: 0004-637X,

1538-4357. DOI: 10.1088/0004-637X/706/1/516. arXiv: 0910.1089 [astro-ph]. (Visited on 03/22/2023).